Ceramics International 46 (2020) 12449–12457

Contents lists available at ScienceDirect

Ceramics International

journal homepage: www.elsevier.com/locate/ceramint

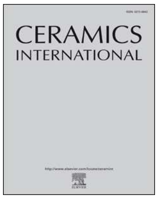

High-pressure synthesis of high-performance submicron-sized polycrystalline β-Si_3N_4 bulk without additives

Zhiqiang Hou[a], Haikuo Wang[a,*], Ya-nan Yang[a], Xudong Song[c], Shuaipeng Chen[d], Shun Wan[b], Xiaomiao Zhao[a], Mengya Shang[a], Bin Chen[b]

[a] *Institute of Materials Pressing Treatment, School of Materials Science and Engineering, Henan University of Technology, Zhengzhou, 450001, China*
[b] *Center for High Pressure Science and Technology Advanced Research, Shanghai, 201203, China*
[c] *Key Lab of Metastable Materials Science & Technology and College of Materials Science & Engineering, Yanshan University, Qinhuangdao, 066004, China*
[d] *School of Materials Science and Engineering, Hunan University, Changsha, 410082, China*

ARTICLE INFO

Keywords:
Micron-sized α-Si_3N_4
Submicron-sized polycrystalline β-Si_3N_4
High pressure and high temperature (HPHT)
Phase transformation
Grain size

ABSTRACT

Dense and submicron-sized polycrystalline β-Si_3N_4 bulk samples with average grain size of 263 ± 68 nm have been synthesized using micron-sized α-Si_3N_4 powder (2 μm) as the starting material by simultaneously tuning the pressure and temperature conditions. The measured Vickers hardness H_V of the submicron-sized polycrystalline β-Si_3N_4 could reach up to about 20 GPa, approaching the upper limit of the single crystal β-Si_3N_4. The measured fracture toughness K_{IC} of the polycrystalline β-Si_3N_4 has been enhanced from 3.0 to 4.1 MPa $m^{1/2}$, as much as 36%, while without sacrificing the hardness. This study demonstrates that using micron-sized powder as the starting material to synthesize submicron-sized polycrystalline bulks by phase transformation under extreme pressure conditions is an efficient pathway to break through the old paradigm—the higher the fracture toughness of a material, the lower the hardness.

1. Introduction

Silicon nitride (Si_3N_4) ceramics are one of the most promising high-temperature materials for structural and technological applications due to its high-temperature excellent thermal stability, good corrosion resistance, and superior mechanical properties [1–3]. However, dense β-Si_3N_4 bulk materials are very difficult to obtain without high pressure or sintering additives because of its Si–N strong covalent bonding and low self-diffusion coefficients [4,5]. In general, there are several conventional methods were used to fabricate β-Si_3N_4 materials such as hot pressing [6,7], hot isostatic press sintering (HIP) [8–13], oscillatory pressure sintering [14,15], spark plasma sintering [16], and microwave heating sintering [17–21]. Moreover, the densification of β-Si_3N_4 ceramic materials is usually achieved by liquid-phase sintering with the aid of oxide additives such as Al_2O_3, MgO, ZrO_2, and Y_2O_3. However, the grain-boundary glassy phase resulting from the sintering additives generally degrades the high-temperature mechanical properties and oxidation resistance of β-Si_3N_4 materials, which inhibits their applications in harsh environments [1,2].

No-additive sintering is another approach to obtain dense β-Si_3N_4 materials. Homma et al. [9] reported α-Si_3N_4 powder could be densified without the use of oxide additives by HIP and obtained the sintered β-Si_3N_4 materials with more than 99% relative density. Tanaka et al. [10,11] demonstrated the feasibility of densifying high-purity α-Si_3N_4 above 1900 °C by HIP and indicated that the mechanical properties of the sintered β-Si_3N_4 bodies were strongly dependent on the impurity content and sintering condition. They also fabricated a fully dense β-Si_3N_4 bulk material with a mean grain size of about 0.7 μm using nanosized α-Si_3N_4 powder (0.1 μm) as a starting material and reported Vickers hardness of about 19 GPa and indentation fracture toughness of 3.0 MPa $m^{1/2}$ [12]. Lu et al. [13] sintered amorphous exposed Si_3N_4 powder (16.7 nm) without any additives at 1950 °C by HIP and obtained extremely dense and high-purity β-Si_3N_4 sample which has a great amount of lath-like or needle-like β-Si_3N_4 grains with a mean size of 500 nm. The minimum grain size of the pure β-Si_3N_4 materials obtained so far is about 500 nm because conventional methods for synthesizing fully dense β-Si_3N_4 materials without additives require sintering temperatures that exceed 1900 °C, this requirement induces β-Si_3N_4 grain growth that consequently causes the disappearance of fine grains (nanostructures and submicron structures) and the degradation of mechanical properties [9–13,22]. Therefore, it is still a challenge to synthesize fine-grained polycrystalline β-Si_3N_4 bulk materials with good mechanical properties by conventional sintering methods.

Reducing the grain size has been the most widely used approach for

---

[*] Corresponding author.
E-mail address: haikuo.wang@zju.edu.cn (H. Wang).

https://doi.org/10.1016/j.ceramint.2020.02.007
Received 23 September 2019; Received in revised form 29 January 2020; Accepted 1 February 2020

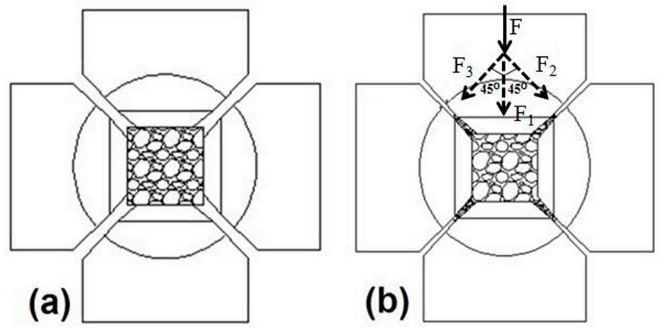

Fig. 1. Schematic diagram of the high-pressure device in large volume cubic press: (a) Pressure medium at the beginning and (b) at the end of the pressurizing stroke.

enhancing hardness and fracture toughness in fine-grained polycrystalline bulk materials such as nano- and submicron polycrystalline diamond and cubic boron nitride [23–28], nanotwinned diamond and cubic boron nitride [29,30], and submicron polycrystalline tetragonal ZrO_2 and cubic Si_3N_4 [31,32]. High pressure and high temperature (HPHT) conditions are necessary for synthesizing fine-grained polycrystalline bulk materials because high temperature enhances the nucleation rate, and high pressure facilitates the densification of the residual porosity and suppresses grain growth by reducing the atomic diffusion responsible for crystallization [23,28,30]. In the present study, micron-sized α-Si_3N_4 starting powder without additives was sintered by HPHT at a pressure of 5.5 GPa and temperatures ranging of 1600–1900 °C. The phase contents, microstructures, and mechanical properties of the synthetic polycrystalline β-Si_3N_4 bulk samples were studied.

2. Experimental

2.1. Starting material

Micron-sized α-Si_3N_4 powder with a mean grain size of 2 μm was used as the starting material (Shanghai Xiangtian Nano Materials Co., Ltd, China). The starting powder was dried in a vacuum oven at 200 °C for 12 h and then pressed into cylindrical green pellets coated by molybdenum layer of a thickness of 0.076 mm through die-pressing at 500 MPa.

2.2. HPHT sintering

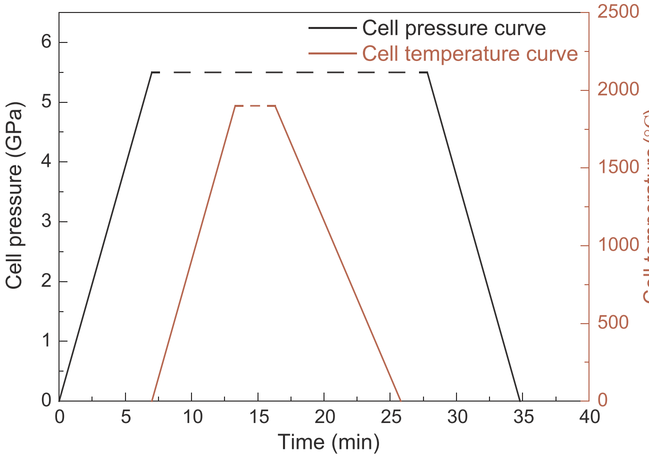

Fig. 3. Schematic of sintering at 5.5 GPa and 1900 °C for 3 min.

The pressed α-Si_3N_4 compact samples were sintered in a 6 × 8 MN large-volume cubic-type multi-anvil apparatus. The schematic diagram of the high-pressure device in large volume cubic press is shown in Fig. 1. To operate the cubic press, six WC anvils are fixed on six pistons and simultaneously pushed by six hydraulic cylinders. The six anvils define a center cubic cavity, inside of which is the cubic assembly in our experiments, as shown in Fig. 2. The motion of the six anvils compresses the cubic assembly, so that the sample chamber pressure continues to build up in the assembly with a decrease in the volume of the pyrophyllite cube. The treating temperature of the sample chamber was calibrated by Type C W–Re thermocouples. The pressure was estimated using the pressure-induced phase transformation of Bi, Tl, and Ba: Bi has two well-known phase transitions at 2.55 and 7.7 GPa, Tl has one at 3.67 GPa, and Ba has one at 5.5 GPa. The more detailed descriptions of the pressure and temperature calibration utilized in this research were presented elsewhere [33,34]. In the HPHT sintering experiments, green compacts were gradually compressed to 5.5 GPa at ambient temperature, and then the temperature was stepwise increased with a heating rate of about 300 °C/min to the desired value. The duration of heating was 3–15 min. The samples were quenched at a rate of about 200 °C/min and then slowly decompressed. To facilitate understanding the high pressure and high temperature experimental process, a schematic of sintering at 5.5 GPa and 1900 °C for 3 min is shown in Fig. 3.

2.3. Characterization

The grain size distribution of the α-Si_3N_4 starting powder was determined using a laser particle size analyzer (Microtrac S3000, USA).

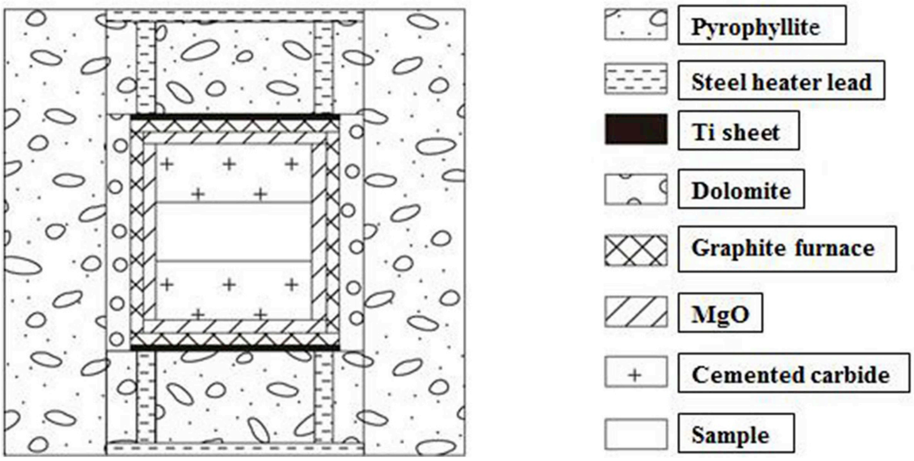

Fig. 2. Schematic diagram of the sample assembly part in high-pressure experiments.

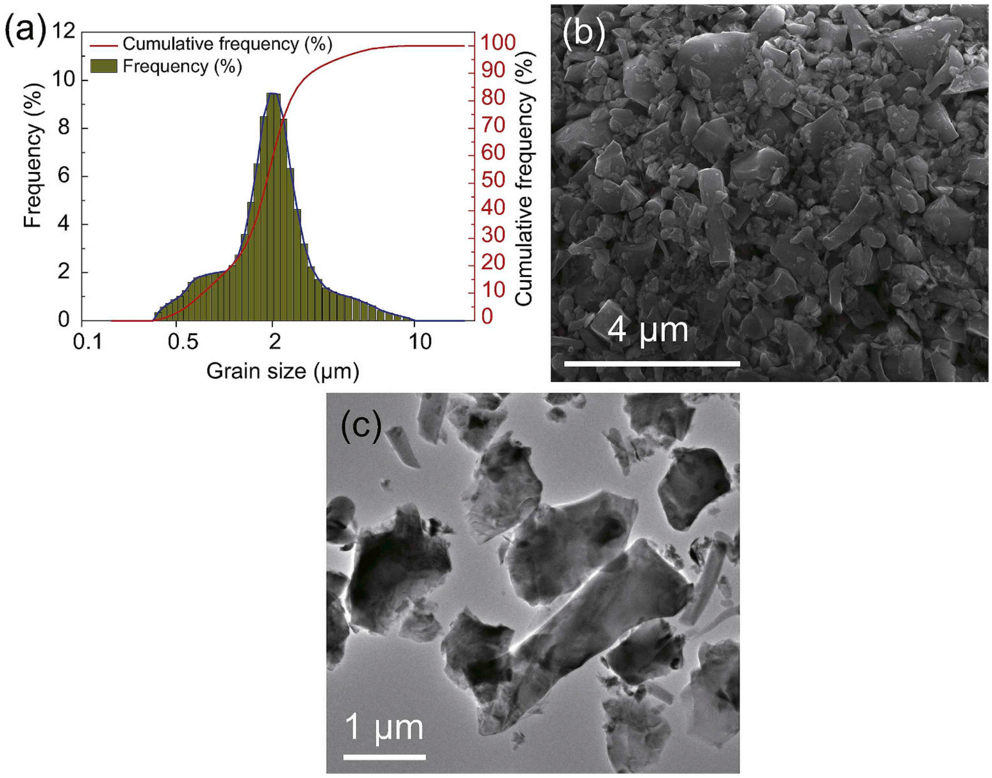

Fig. 4. (a) Grain size and cumulative size distribution of the α-Si_3N_4 starting powder. (b) SEM image of the α-Si_3N_4 powder. (c) Brightfield TEM micrograph of the α-Si_3N_4 starting powder.

Table 1
Characteristics of the α-Si_3N_4 starting material.

α-Si_3N_4 content (%)	Mean grain size (μm)	Impurities (wt.%)				
		C	O	Fe	Cr	Al
> 95	2	< 0.002	< 0.27	< 0.009	< 0.002	< 0.1

The starting powder was dispersed in water and exposed to ultrasounds during analysis. The morphology and grain size of the starting powder and the microstructure of the sintered samples were examined by scanning electron microscope (SEM, FEI INSPECT F50, USA) and field-emission transmission electron microscope (TEM, FEI Tecnai G^2 F30, USA). The phase identification and structural characterization of the starting powder and the recovered sintered samples were performed using an X-ray diffractometer (XRD, D8 Advance, Germany) utilizing Cu Kα radiation. The relative amounts of the α- and β-Si_3N_4 in the sintered samples were calculated from the equation of the peak intensities of (210) plane diffractions reported by Gazzara and Messier [35]. Raman scattering spectra were obtained at room temperature in a confocal Raman system utilizing a solid-state laser (532 nm, Nd: Yag laser, HORIBA Jobin Yvon, France). The bulk density of the sintered samples was measured by the Archimedes method. The sintered specimens were polished with diamond slurry, and then etched with a mixture of HF and HNO_3 (1:1) at 70 °C. Room temperature ultrasonic measurements were performed for the bulk samples by a pulse-echo method with an advanced ultrasonic material characterization system (UMS-100, TECLAB, France). The Vickers hardness of the end-polished samples was measured using a Vickers hardness tester (FM-ARS 900, Future-Tech, Japan). The fracture toughness of the same specimens was assessed by the indentation method with a load of 9.8 N and a dwell time of 15 s.

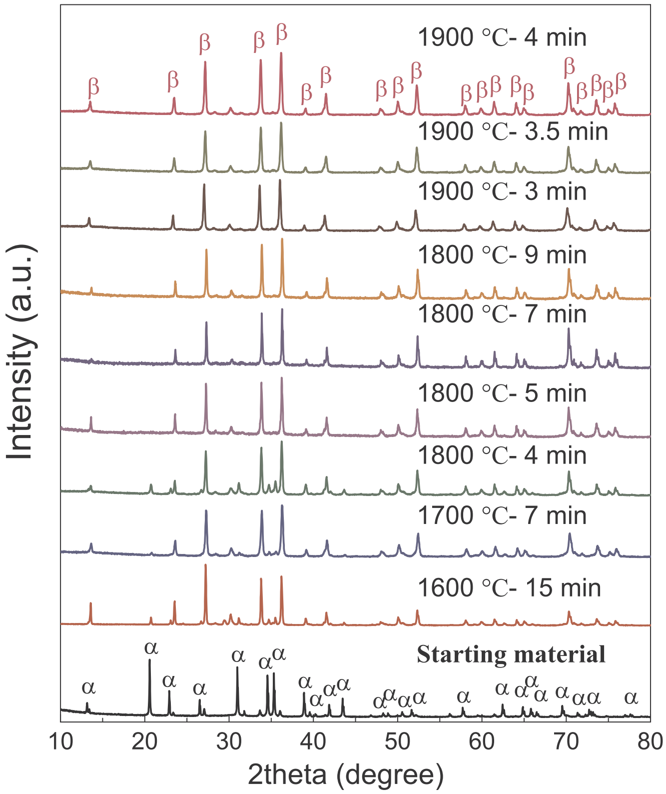

Fig. 5. XRD patterns of the starting material and the recovered products synthesized at 5.5 GPa and 1600–1900 °C.

Table 2

XRD intensity ratios of α- and β-Si_3N_4 of the recovered samples as a function of sintering temperature (*T*, °C) and holding time (*t*, min).

T (°C)	*t* (min)	$\beta_{(210)}/(\beta_{(210)}+\alpha_{(210)})$
1600	15	0.88
1700	7	0.94
1800	4	0.82
1800	5	1
1800	7	1
1800	9	1
1900	3	1
1900	3.5	1
1900	4	1

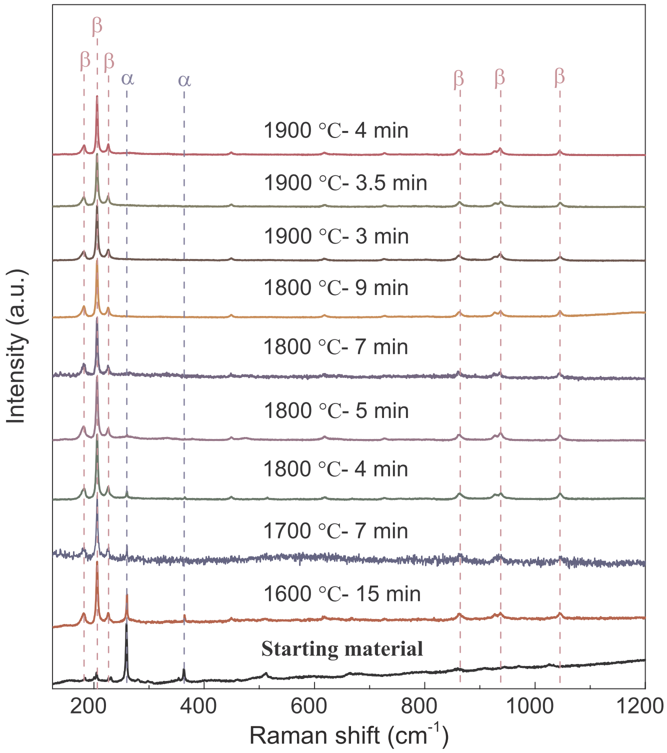

Fig. 6. Raman spectra patterns of the starting material and the samples sintered at 5.5 GPa and 1600–1900 °C.

3. Results and discussion

3.1. Micron-sized powder characterization

The grain size distribution of the α-Si_3N_4 starting powder is shown in Fig. 4(a). The α-Si_3N_4 powder displays a multi-modal narrow grain size distribution, ranging from 0.4 to 10 μm. The major micrometric population corresponds to the primary grains observed in SEM image with a size centered at 2 μm [Fig. 4(b)]. The TEM micrograph of the α-Si_3N_4 starting powder is presented in Fig. 4(c). Morphology and grain size are in close agreement with SEM observation. The characteristics of the starting material are shown in Table 1.

3.2. Phase transformation and microstructure

Fig. 5 shows the XRD patterns of the starting material and the recovered samples synthesized at a pressure of 5.5 GPa and temperatures ranging of 1600–1900 °C for different holding time. As clearly seen from Fig. 5, the X-ray pattern analysis of the starting material revealed hexagonal α-Si_3N_4 as the major phase. Moreover, the phase transformation from α-Si_3N_4 to β-Si_3N_4 was incomplete at temperatures below 1700 °C. Full transformation was not attained even at 1800 °C for 4 min and was obtained at 1800 °C for 5 min (i.e. no α-Si_3N_4 phase was detected in the sample). Full transformation also was observed at 1900 °C for 3 min. In addition, an unknown weak and tiny peak at 2θ = 30.3° was detected in all sintered samples. Table 2 lists the XRD intensity ratios of the α- and β-Si_3N_4 of the recovered polycrystalline β-Si_3N_4 bulk samples.

Fig. 6 shows the Raman spectra patterns of the starting material and the recovered samples sintered at 5.5 GPa and 1600–1900 °C. The results of Raman spectra analysis were in good agreement with the XRD patterns. Bradley et al. [36] reported that the full transformation from α-Si_3N_4 to β-Si_3N_4 could be observed at 5 GPa and 2000 °C for 6 min without mineralizer additives. However, full phase transformation from α-Si_3N_4 to β-Si_3N_4 in this study occurred at 1800 °C, which was about 200 °C lower than that of previous research.

Fig. 7 shows TEM images of the polycrystalline β-Si_3N_4 sample sintered at 5.5 GPa and 1900 °C for 3 min. Fig. 7(b) and (c) show high-resolution TEM (HRTEM) images of the sample. It can be seen that HRTEM images showed clean grain boundaries (i.e. no intergranular phase, crystalline or glassy, was ever detected), which is characteristic of no eutectic liquid-phase sintering [13]. HRTEM observation showed that full phase transformation from α-Si_3N_4 to β-Si_3N_4 could be completed without eutectic liquid phase. Moreover, the temperature of the full phase transformation is close to the melting point of silicon nitride, which is about 1900 °C under high pressure [1,18]. Therefore, we speculated that the molten liquid Si_3N_4 phase could be formed when the temperature reached or approached the melting point of α-Si_3N_4, and then the β-Si_3N_4 crystals will be formed by the nucleation-growth mechanism of liquid-solid phase transformation. In addition, HPHT conditions can accelerate phase transformation from α-Si_3N_4 to β-Si_3N_4 [36].

The well-sintered recovered samples are cylinder-shaped chunks that are about 11 mm in diameter and 4 mm in height after polishing (Fig. 8). Fig. 9 shows SEM images of the submicron-sized polycrystalline β-Si_3N_4 bulk specimens synthesized at 1800 °C and 1900 °C under a pressure of 5.5 GPa. It can be seen that all recovered samples show a dense microstructure and lacked microcracks, indicating that the β-Si_3N_4 crystals were well bonded by the submicron-sized grains. The microstructures of the samples show equiaxed grains, regular in shape.

The mean grain size of polycrystalline β-Si_3N_4 bulk samples was measured from the linear length of grains, and a minimum of 200 grains were counted for each specimen. Grain size distribution of bulk samples of full transformation shows a relatively narrow range in submicron size (Fig. 10). The mean grain sizes of samples produced at 1800 °C for 5, 7, and 9 min are 268 ± 78, 298 ± 77, and 342 ± 86 nm, respectively, whereas those of samples produced at 1900 °C for 3, 3.5, and 4 min are 263 ± 68, 272 ± 105, and 352 ± 108 nm, respectively. In this study, the minimum mean grain size after full transformation is 263 ± 68 nm, which is much smaller than that reported in previous literatures [10,16,18,21].

3.3. Mechanical properties

The hardness values reported were the average of 10 different measurements. The test results show that the hardness decreases with the loading force increases [Fig. 11(a)], and the H_V-F load curve eventually bends over and levels off at higher loads which have been extensively documented in many different types of hard and brittle materials previously [26–30,32,37–39]. This phenomenon may be attributed to the indentation size effect. In the present study, we employed H_V at 4.9 N as a reference value for the polycrystalline β-Si_3N_4 bulk samples because H_V shows an asymptotic value when the load was 4.9 N or higher.

Fig. 11 (b) shows the micrograph of the Vickers indentation of the submicron-sized polycrystalline β-Si_3N_4 bulk obtained at 5.5 GPa and 1900 °C for 3.5 min. The size of the Vickers indentation was

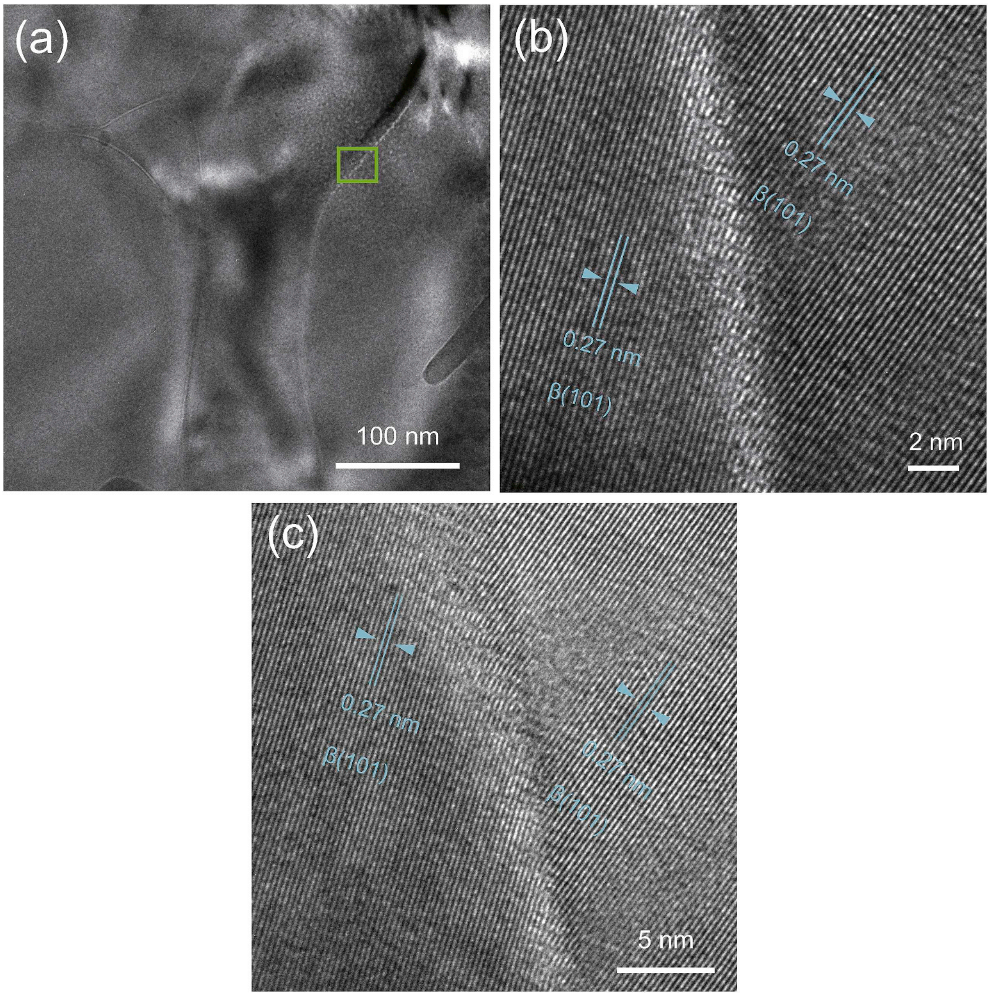

Fig. 7. TEM images of the polycrystalline β-Si_3N_4 sample sintered at 5.5 GPa and 1900 °C for 3 min. (a) Low-magnification TEM image the sample. (b) and (c) HRTEM images of the area marked with the green box in (a). (For interpretation of the references to colour in this figure legend, the reader is referred to the Web version of this article.)

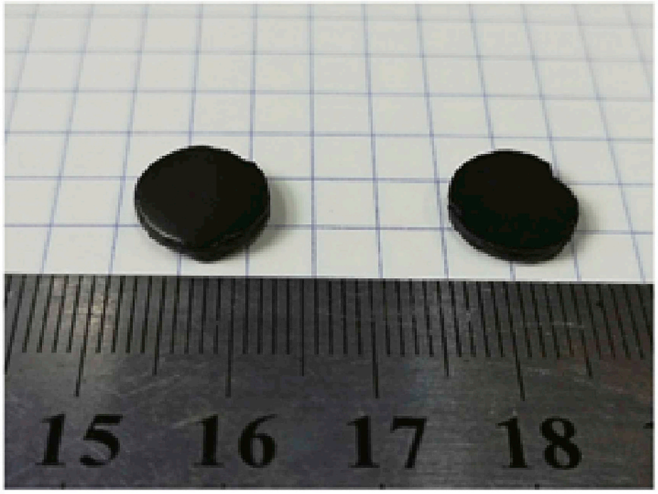

Fig. 8. Optical microscope image of submicron-sized polycrystalline β-Si_3N_4 bulk samples (about 11 mm in diameter and 4 mm in height).

substantially larger (by more than a factor of 20) than the grain size of the submicron polycrystalline β-Si_3N_4 sample, indicating the measured hardness is meaningful and represented the hardness of the submicron polycrystalline β-Si_3N_4 bulk rather than the single crystal β-Si_3N_4 grain [8]. As the load was increased from 0.49 to 4.9 N, the average hardness decreased from 24.6 ± 1.0 to 19.9 ± 0.6 GPa, with a maximum measured hardness of 20.9 GPa under 4.9 N of load. In addition, no visible microcrack was observed until the load reached up to 4.9 N. In order to guarantee the credibility of our fracture toughness test, we measured the fracture toughness of the bulk samples at the load of 9.8 N, which appearance noticeable propagation of microcracks.

Grain size has a very pronounced effect on the hardness and fracture toughness, especially for polycrystalline bulk materials with grain size in submicron-sized or nanosized range [40]. Fig. 12 shows that H_V as a function of the grain size of fully transformed submicron-sized polycrystalline β-Si_3N_4 bulk samples. The H_V versus grain size curve shows that the H_V increases monotonically as the grain size decreases, which comply with the Hall-Petch effect [41,42]. Greskovich et al. [8] indicated that the hardness of pure single crystal β-Si_3N_4 is the upper limit of the full-density single-phase polycrystalline β-Si_3N_4 materials. In this study, the measured hardness of the recovered sample synthesized at 5.5 GPa and 1900 °C for 3 min could reach up to about 20 GPa which is the upper limit of the single crystal β-Si_3N_4 [43].

The longitudinal and transverse sound velocities of the submicron-sized polycrystalline β-Si_3N_4 bulk samples were measured using a pulse-echo method. Values for Young's modulus (E), bulk modulus (B), shear modulus (G), and Poisson's ratio (v) were calculated from the density of the sintered bulk samples, together with the longitudinal and transverse velocities of the acoustic waves [44,45]. The fracture

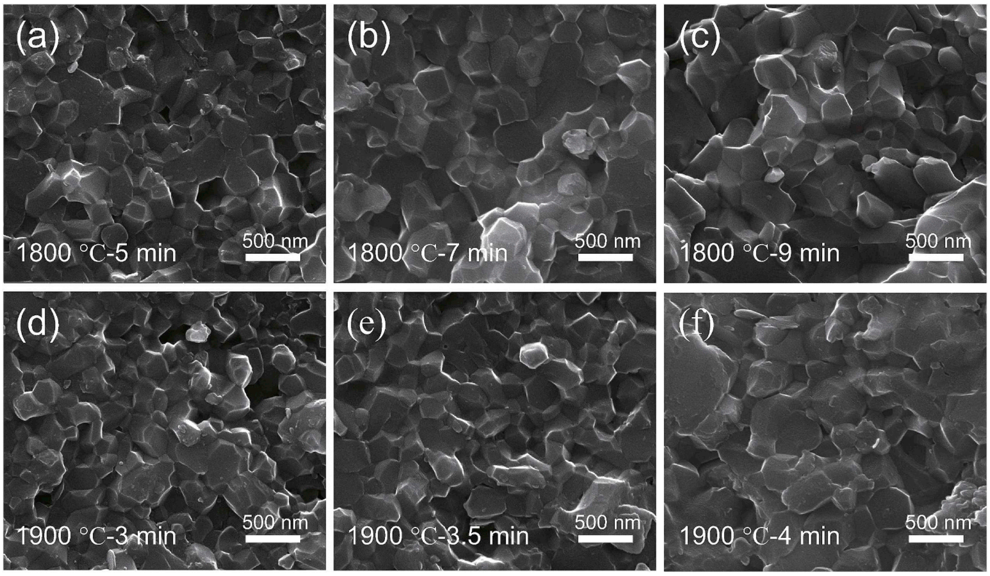

Fig. 9. SEM images of the submicron-sized polycrystalline β-Si_3N_4 bulk samples synthesized at 5.5 GPa and (a) 1800 °C for 5 min, (b)1800 °C for 7 min, (c) 1800 °C for 9 min, (d) 1900 °C for 3 min, (e) 1900 °C for 3.5 min, and (f) 1900 °C for 4 min.

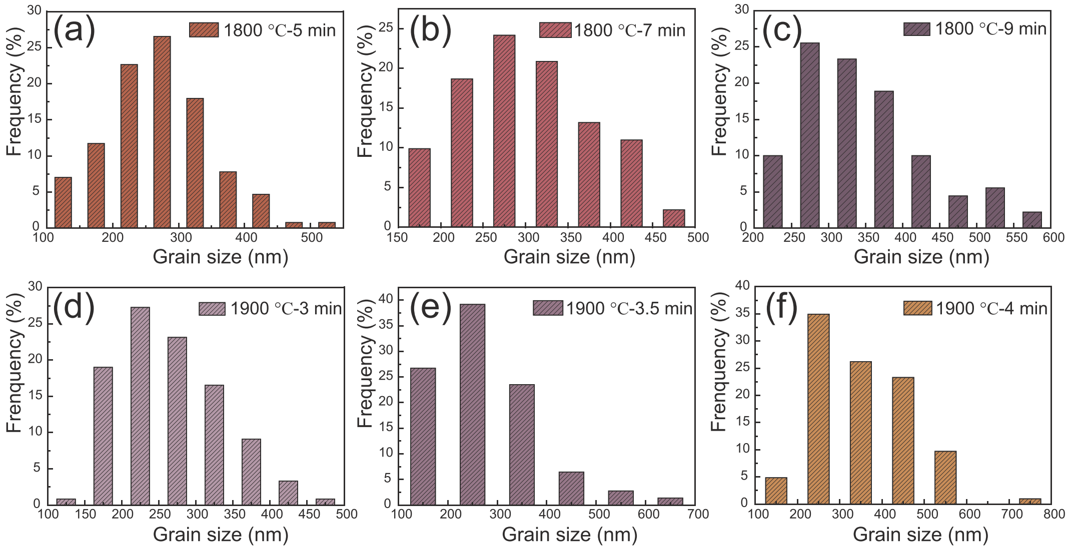

Fig. 10. Grain size distribution of submicron-sized polycrystalline β-Si_3N_4 bulk samples obtained at 5.5 GPa and 1800–1900 °C.

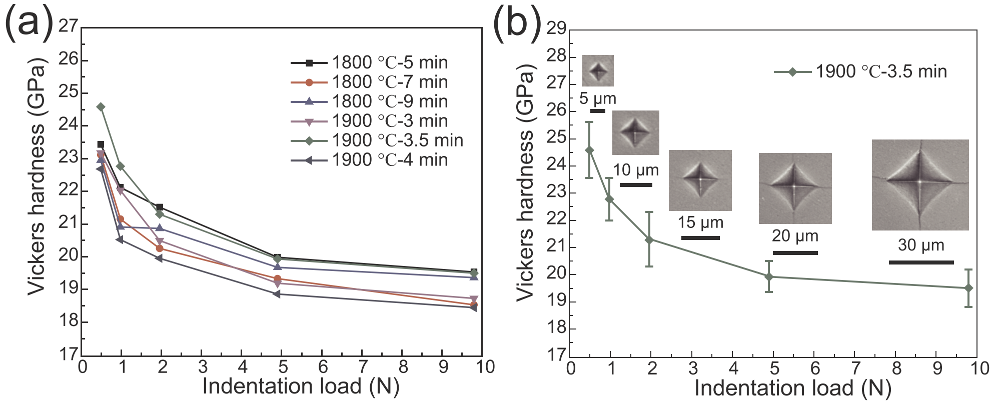

Fig. 11. (a) Vickers hardness H_V of submicron-sized polycrystalline β-Si_3N_4 bulk specimens as a function of applied load. (b) H_V-F load curve of the sample obtained at 5.5 GPa and 1900 °C for 3.5 min. Insets present the Vickers indentation under different loads.

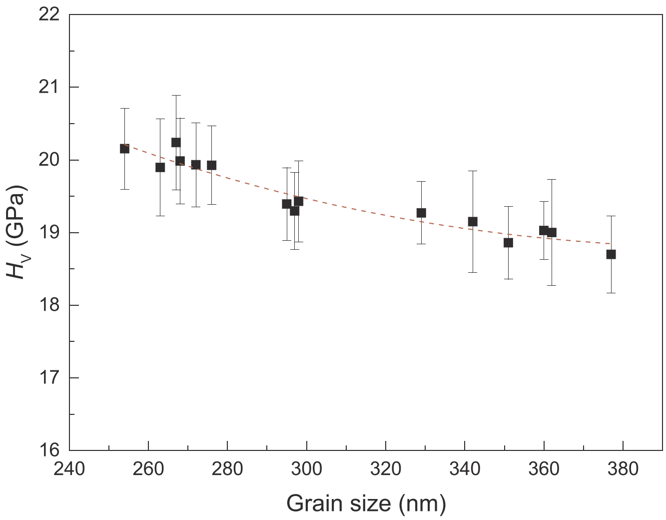

Fig. 12. H_V as a function of the grain size of fully transformed submicron-sized polycrystalline β-Si_3N_4 bulk specimens produced at 5.5 GPa and 1800–1900 °C.

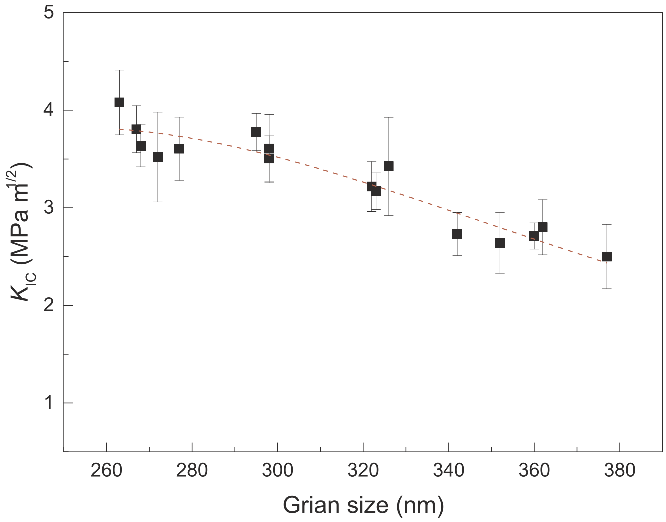

Fig. 13. K_{IC} as a function of the grain size of fully transformed submicron-sized polycrystalline β-Si_3N_4 bulk samples produced at 5.5 GPa and 1800–1900 °C.

toughness of submicron-sized polycrystalline β-Si_3N_4 bulk samples under a load of 9.8 N was calculated on the basis of the following equation [46,47]:

$$K_{IC} = \xi\,(E / H_V)^{1/2}\,(P / c^{3/2})$$

where ξ is a calibration constant of 0.0166 ± 0.004, E is the Young's modulus (GPa), H_V is the hardness (GPa), P is the loading force (N), and c is the crack length. The crack lengths were measured using optical microscope after making indentation on the polished samples.

Fig. 13 shows that K_{IC} as a function of the grain size of fully transformed submicron-sized polycrystalline β-Si_3N_4 bulk samples. As can be seen, the measured fracture toughness K_{IC} of the synthesized submicron-sized polycrystalline β-Si_3N_4 samples increases greatly, as much as 55%, as the β-Si_3N_4 grain size decreases from 377 ± 110 to 263 ± 68 nm, while without sacrificing the hardness. The achieved highest K_{IC} of 4.1 MPa $m^{1/2}$ for the polycrystalline β-Si_3N_4 bulk samples without additives synthesized at 5.5 GPa and 1900 °C for 3 min is 36% tougher than the β-Si_3N_4 compact without additives (K_{IC}~3.0 MPa $m^{1/2}$) obtained at 1950 °C for 2 h by HIP [10]. Our data on the fracture toughness versus the grain size of the polycrystalline β-Si_3N_4 bulk samples also show a good fit to the Hall-Petch effect. The above results provide experimental evidence for the submicron-sized effect on the fracture toughness of polycrystalline bulk materials.

Table 3 shows our results of the density (ρ), Vickers hardness (H_V), fracture toughness (K_{IC}), Young's modulus (E), bulk modulus (B), shear modulus (G), and Poisson's ratio (ν) of the submicron-sized polycrystalline β-Si_3N_4 bulk samples synthesized at 5.5 GPa and different temperatures (T) for selected holding time (t).

Fracture mechanics studies have suggested that the morphology and grain size are the key factors for the process of crack deflection and propagation [48]. Fig. 14 shows the indentation crack profiles in the recovered samples. As is clearly seen from this figure that the fracture mode was predominantly intergranular fracture with obvious crack deflection, this phenomenon indicating that bonding strength between adjacent β-Si_3N_4 grains is weaker than the single crystalline. Tanaka et al. [12] reported that an indentation fracture toughness of 3.5 ± 0.4 MPa $m^{1/2}$ for β-Si_3N_4–20 vol% β-Si_3N_4 whisker composite synthesized without sintering additives and observed that the crack cuts the whisker and predominantly propagates transgranularly, their study indicated that the whisker did not contribute much to the fracture toughness. Large grains have a negligible effect on mechanical properties because toughening mechanisms in β-Si_3N_4 ceramics depend on the generation of numerous tortuous crack paths with intergranular fractures [18,49]. The simultaneous improvement in the hardness and fracture toughness of the polycrystalline β-Si_3N_4 bulk ceramics in our study is intimately related to the ubiquitous submicron-sized microstructures. The presence of fine submicron-sized grains introduces extra hardening as a result of the Hall-Petch effect at the submicron-sized scale, whereas the propagation of microcracks along densely distributed grain boundaries enhances fracture toughness [29,30,40]. In our present study, as the β-Si_3N_4 grains become smaller, the effect of restricting crack propagation increases, thereby toughening the polycrystalline β-Si_3N_4 materials.

In many cases, polycrystalline β-Si_3N_4 bulk materials synthesized by conventional methods cannot reach to the exceptional hardness and fracture toughness. The reason is that the nanosized or submicron-sized α-Si_3N_4 precursors direct sintering at room pressure unavoidably lead to the grain growth, which to a large extent degrade the mechanical properties of polycrystalline β-Si_3N_4 ceramics. However, in contrast to conventional methods, our approach overcomes the grain-growth problem of polycrystalline β-Si_3N_4 materials. HPHT conditions can facilitate the phase transformation from α-Si_3N_4 to β-Si_3N_4 and suppress β-Si_3N_4 grain growth. The use of micron-sized α-Si_3N_4 powder without additives guarantees the formation of a number of clean grain

Table 3
List of density (ρ), Vickers hardness (H_V), fracture toughness (K_{IC}), Young's modulus (E), bulk modulus (B), shear modulus (G), and Poisson's ratio (ν) of submicron-sized polycrystalline β-Si_3N_4 bulks obtained at 5.5 GPa and different sintering temperature (T) for selected holding time (t).

T (°C)	t (min)	ρ (g·cm^{-3})	H_V (GPa)	K_{IC} (MPa $m^{1/2}$)	E (GPa)	B (GPa)	G (GPa)	ν
1800	5	3.111	19.9 ± 0.6	3.6 ± 0.2	281.7	213.6	110.0	0.280
1800	7	3.100	19.4 ± 0.6	3.6 ± 0.4	295.8	215.8	116.3	0.272
1800	9	3.101	19.2 ± 0.7	2.7 ± 0.2	290.7	213.8	114.2	0.273
1900	3	3.107	19.9 ± 0.7	4.1 ± 0.3	292.5	223.1	114.1	0.282
1900	3.5	3.102	19.9 ± 0.6	3.5 ± 0.5	280.9	221.0	109.0	0.288
1900	4	3.089	18.9 ± 0.5	2.6 ± 0.3	290.9	215.0	114.2	0.274

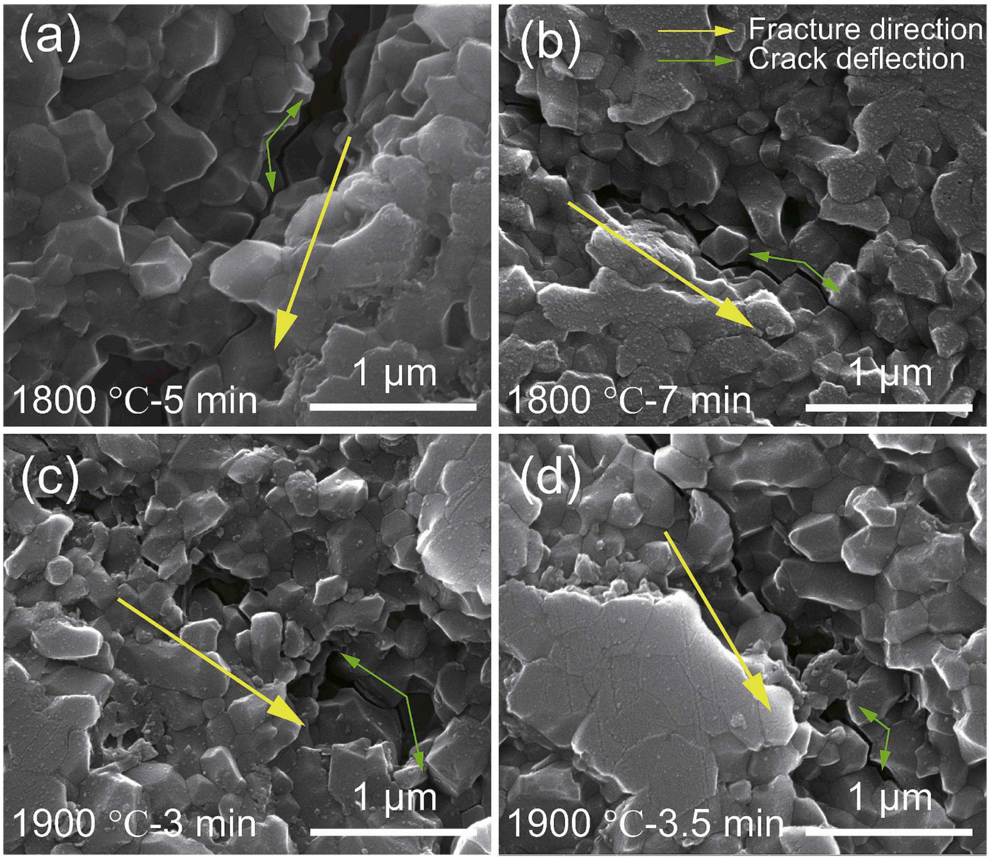

Fig. 14. Indentation crack paths on the polished and etched surface of submicron-sized polycrystalline β-Si_3N_4 bulks sintered at (a) 1800 °C for 5 min, (b)1800 °C for 7 min, (c) 1900 °C for 3 min, and (d) 1900 °C for 3.5 min.

boundaries, which can enhance the bonding strength of β-Si_3N_4 grains. The subtle interplay between extreme pressure, sintering temperature and holding time allows finer controls in formation of submicron-structured polycrystalline β-Si_3N_4 bulk materials. This study demonstrates that under the optimized HPHT conditions (i.e. 5.5 GPa, 1800 °C for 5 min, or 1900 °C for 3 min), the submicron-sized polycrystalline β-Si_3N_4 bulk materials with superior mechanical properties could be synthesized using the micron-sized α-Si_3N_4 powder as the starting material. This synthetic technique provides an efficient method to design and develop good quality submicron-sized or nanosized polycrystalline bulk ceramics.

4. Conclusions

Our experiments proposed a strategy in preparing submicron-sized polycrystalline bulk ceramics. The key to synthesize submicron structures is to choose suitable starting material and appropriate HPHT conditions. In this study, the well-prepared polycrystalline β-Si_3N_4 bulk sample obtained at 5.5 GPa and 1900 °C for 3 min has a mean grain size of 263 ± 68 nm, and the measured hardness is 19.9 ± 0.7 GPa, which achieves the upper limit of the single crystal β-Si_3N_4. Simultaneously the measured fracture toughness reaches up to 4.1 ± 0.3 MPa $m^{1/2}$, which is about 36% tougher than conventional β-Si_3N_4 compact without additives . The reduced grain size contributed to the improved hardness and fracture toughness.

Declaration of competing interest

There are no conflicts of interest to declare.

Acknowledgements

This work was supported by the National Key R&D Program of China (Grant No. 2018YFA0703400), the National Natural Science Foundation for Youth Scholars of China (Grant Nos. 11504087 and 11804307), the Natural Science Foundation of Henan Province (Grant No. 162300410051), and the Science and Technology Directorate Major Project of Zhengzhou (Grant No. 174PZDZX567). The authors also thank Qiuling Chen (Henan University of Technology) for her useful discussion and advice.

References

[1] F.L. Riley, Silicon nitride and related materials, J. Am. Ceram. Soc. 83 (2000) 245–265.
[2] H. Klemm, Silicon nitride for high-temperature applications, J. Am. Ceram. Soc. 93 (2010) 1501–1522.
[3] A. Zerr, G. Miehe, G. Serghiou, M. Schwarz, E. Kroke, R. Riedel, H. Fueß, P. Kroll, R. Boehler, Synthesis of cubic silicon nitride, Nature 400 (1999) 340–342.
[4] D. Hardie, K.H. Jack, Crystal structures of silicon nitride, Nature 180 (1957) 332–333.
[5] I.W. Chen, A. Rosenflanz, A tough SiAlON ceramic based on α-Si_3N_4 with a whisker-like microstructure, Nature 389 (1997) 701–704.
[6] R.J. Sung, T. Kusunose, T. Nakayama, Y.H. Kim, T. Sekino, S. Lee, K. Niihara, Mechanical properties of transparent polycrystalline silicon nitride, Key Eng. Mater. 317–318 (2006) 305–308.
[7] Q.G. Jiang, W.M. Guo, W. Liu, S.X. Gu, L.X. Cheng, J. Liu, M.P. Zhou, S.H. Wu, Influence of powder characteristics on hot-pressed Si_3N_4 ceramics, Sci. Sinter. 49 (2017) 81–89.
[8] C. Greskovich, H.C. Yeh, Hardness of dense β-Si_3N_4, J. Mater. Sci. Lett. 2 (1983) 657–659.
[9] K. Homma, H. Okada, T. Fujikawa, T. Tatuno, HIP sintering of silicon nitride without additives, Yogyo-Kyokai-Shi 95 (1987) 229–234.
[10] I. Tanaka, G. Pezzotti, T. Okamoto, Y. Miyamoto, M. Koizumi, Hot isostatic press sintering and properties of silicon nitride without additives, J. Am. Ceram. Soc. 72 (1989) 1656–1660.
[11] I. Tanaka, G. Pezzotti, T. Okamoto, Y. Miyamoto, M. Koizumi, Dense silicon nitride

without additives: sintering and high temperature behaviors, Ceram. Eng. Sci. Proc. 10 (1989) 817–822.

[12] I. Tanaka, G. Pezzotti, Y. Miyamoto, T. Okamoto, Fracture toughness of Si_3N_4 and its Si_3N_4 whisker composite without sintering aids, J. Mater. Sci. 26 (1991) 208–210.

[13] P. Lu, S.C. Danforth, W.T. Symons, Microstructure and grain-boundary characterization of HIP'ed high-purity silicon nitride, J. Mater. Sci. 28 (1993) 4217–4222.

[14] Y. Han, Z. Xie, S. Li, T. Zhu, W. Wu, D. An, F. Hu, F. Zhai, Optimum sintering temperature of high quality silicon nitride ceramics under oscillatory pressure, Ceram. Int. 44 (2018) 6949–6952.

[15] S. Li, C. Wei, L. Zhou, P. Wang, W. Wang, Microstructure and fracture strength of silicon nitride ceramics consolidated by oscillatory pressure sintering, Ceram. Int. 45 (2019) 15671–15675.

[16] M. Hotta, T. Shinoura, N. Enomoto, J. Hojo, Spark plasma sintering of nanosized amorphous silicon nitride powder with a small amount of sintering additives, J. Am. Ceram. Soc. 93 (2010) 1544–1546.

[17] M.I. Jones, M.C. Valecillos, K. Hirao, M. Toriyama, Densification behavior in microwave-sintered silicon nitride at 28 GHz, J. Am. Ceram. Soc. 84 (2001) 2424–2426.

[18] M.I. Jones, M.C. Valecillos, K. Hirao, Y. Yamauchi, Grain growth in microwave sintered Si_3N_4 ceramics sintered from different starting powders, J. Eur. Ceram. Soc. 22 (2002) 2981–2988.

[19] O.I. Getman, V.V. Holoptsev, V.V. Panichkina, I.V. Plotnikov, V.K. Soolshenko, Mechanical properties of microwave sintered Si_3N_4-based ceramics, Sci. Sinter. 34 (2002) 223–229.

[20] S. Chockalingam, D.A. Earl, V.R.W. Amarakoon, Phase transformation and densification behavior of microwave-sintered Si_3N_4–Y_2O_3–MgO–ZrO_2 system, Int. J. Appl. Ceram. Technol. 6 (2009) 102–110.

[21] S. Chockalingam, D.A. Earl, Mechanical properties of 2.45 GHz microwave sintered Si_3N_4–Y_2O_3–MgO–ZrO_2 system, J. Eur. Ceram. Soc. 29 (2009) 2037–2043.

[22] A.V. Galakhov, Agglomerates in nanopowders and ceramic technology, Refract. Ind. Ceram. 50 (2009) 348–353.

[23] T. Irifune, A. Kurio, S. Sakamoto, T. Inoue, H. Sumiya, Materials: ultrahard polycrystalline diamond from graphite, Nature 421 (2003) 599–600.

[24] H. Sumiya, K. Harano, Y. Ishida, Mechanical properties of nano-polycrystalline cBN synthesized by direct conversion sintering under HPHT, Diam. Relat. Mater. 41 (2014) 14–19.

[25] J. Lu, Z. Kou, T. Liu, L. Zhang, W. Ding, Q. Zhang, Q. Wang, M. Yang, H. Gong, D. He, Sub-micron polycrystalline diamond synthesis under high temperature and high pressure, Chin. J. High Press. Phys. 32 (2018) 023302.

[26] G. Liu, Z. Kou, X. Yan, L. Lei, F. Peng, Q. Wang, K. Wang, P. Wang, L. Li, Y. Li, W. Li, Y. Wang, Y. Bi, Y. Leng, D. He, Submicron cubic boron nitride as hard as diamond, Appl. Phys. Lett. 106 (2015) 121901.

[27] N. Dubrovinskaia, V.L. Solozhenko, N. Miyajima, V. Dmitriev, O.O. Kurakevych, L. Dubrovinsky, Superhard nanocomposite of dense polymorphs of boron nitride: noncarbon material has reached diamond hardness, Appl. Phys. Lett. 90 (2007) 101912.

[28] V.L. Solozhenko, O.O. Kurakevych, Y.L. Godec, Creation of nanostructures by extreme conditions: high-pressure synthesis of ultrahard nanocrystalline cubic boron nitride, Adv. Mater. 24 (2012) 1540–1544.

[29] Q. Huang, D. Yu, B. Xu, W. Hu, Y. Ma, Y. Wang, Z. Zhao, B. Wen, J. He, Z. Liu, Y. Tian, Nanotwinned diamond with unprecedented hardness and stability, Nature 510 (2014) 250–253.

[30] Y. Tian, B. Xu, D. Yu, Y. Ma, Y. Wang, Y. Jiang, W. Hu, C. Tang, Y. Gao, K. Luo, Z. Zhao, L. Wang, B. Wen, J. He, Z. Liu, Ultrahard nanotwinned cubic boron nitride, Nature 493 (2013) 385–388.

[31] B. Dong, H. Wang, F. Tong, Z. Hou, Z. Li, T. Liu, J. Zang, X. Yang, Fabrication of submicron tetragonal polycrystalline ZrO_2 by the transformation of micro monoclinic ZrO_2 under high pressure, Chin. J. High Press. Phys. 33 (2019) 020104.

[32] N. Nishiyama, R. Ishikawa, H. Ohfuji, H. Marquardt, A. Kurnosov, T. Taniguchi, B.N. Kim, H. Yoshida, A. Masuno, J. Bednarcik, E. Kulik, Y. Ikuhara, F. Wakai, T. Irifune, Transparent polycrystalline cubic silicon nitride, Sci. Rep. 7 (2017) 44755.

[33] H. Wang, D. He, N. Tan, W. Wang, J. Wang, H. Dong, H. Ma, Z. Kou, F. Peng, X. Liu, S. Li, Note: an anvil-performed gasket system to extend the pressure range for large volume cubic presses, Rev. Sci. Instrum. 81 (2010) 116101.

[34] H. Wang, D. He, X. Yan, C. Xu, J. Guan, N. Tan, W. Wang, Quantitative measurements of pressure gradients for the pyrophyllite and magnesium oxide pressure-transmitting mediums to 8 GPa in a large-volume cubic cell, High Pres. Res.: Int. J. 31 (2011) 581–591.

[35] C.P. Gazzara, D.R. Messier, Determination of phase content of by X-ray diffraction analysis, Am. Ceram. Soc. Bull. 56 (1977) 777–780.

[36] R.S. Bradley, D.C. Munro, M. Whitfield, The reactivity and polymorphism of selected nitrides at high temperatures and high pressures, J. Inorg. Nucl. Chem. 28 (1966) 1803–1812.

[37] Y. Zhao, J. Qian, L.L. Daemen, C. Pantea, J. Zhang, G.A. Voronin, T.W. Zerda, Enhancement of fracture toughness in nanostructured diamond-SiC composites, Appl. Phys. Lett. 84 (2004) 1356.

[38] H.Y. Chung, M.B. Weinberger, J.B. Levine, A. Kavner, J.M. Yang, S.H. Tolbert, R.B. Kaner, Synthesis of ultra-incompressible superhard rhenium diboride at ambient pressure, Science 316 (2007) 436–439.

[39] H. Wang, D. He, C. Xu, M. Tang, Y. Li, H. Dong, C. Meng, Z. Wang, W. Zhu, Nanostructured diamond-TiC composites with high fracture toughness, J. Appl. Phys. 113 (2013) 043505.

[40] S. Yip, Nanocrystals: the strongest size, Nature 391 (1998) 532–533.

[41] E.O. Hall, The deformation and ageing of mild steel: III Discussion of results, Proc. Phys. Soc. B 64 (1951) 747–753.

[42] N.J. Petch, The cleavage strength of polycrystals, Journal of the Iron and Steel Institute 174 (1953) 25–28.

[43] D. Chakraborty, J. Mukerji, Characterization of silicon nitride single crystals and polycrystalline reaction sintered silicon nitride by microhardness measurements, J. Mater. Sci. 15 (1980) 3051–3056.

[44] L.G. Hwa, Y.J. Wu, W.C. Chao, C.H. Chen, Pressure- and temperature-dependence of elastic properties of a ZBLAN glass, Mater. Chem. Phys. 74 (2002) 160–166.

[45] S.F. Wang, Y.F. Hsu, J.C. Pu, J.C. Sung, L.G. Hwa, Determination of acoustic wave velocities and elastic properties for diamond and other hard materials, Mater. Chem. Phys. 85 (2004) 432–437.

[46] M.H. Lewis, R. Fung, D.M.R. Taplin, Indentation plasticity and fracture of Si_3N_4 ceramics alloys, J. Mater. Sci. 16 (1981) 3437–3446.

[47] G.R. Anstis, P. Chantikul, B.R. Lawn, D.B. Marshall, A critical evaluation of indentation techniques for measuring fracture toughness: I, direct crack measurements, J. Am. Ceram. Soc. 64 (1981) 533–538.

[48] J.B. Wachtman, W.R. Cannon, M.J. Matthewson, Mechanical Properties of Ceramics, Wiley, 1996, pp. 199–210.

[49] Y. Zhou, H. Hyuga, D. Kusano, Y. Yoshizawa, K. Hirao, A tough silicon nitride ceramic with high thermal conductivity, Adv. Mater. 23 (2011) 4563–4567.